*Pol. J. Environ. Stud. Vol. XX, No. X (XXXX), 1–12*
DOI:*10.15244/pjoes/188453* ONLINE PUBLICATION DATE:

*Original Research*

# Photosynthetic Responses of Two Plant Species on Karst Highway Slopes During Drought in Guangxi, China

**Xu Li[1], Yongke Wei[1], Jiaqing Liu[1], Jie Ma[2, 3], Qukan Luo[2, 3], Fen Huang[2, 3]***

[1]Guangxi Xinfazhan Communication Group Co., Ltd, Nanning 530029
[2]Institute of Karst Geology, CAGS/Key Laboratory of Karst Dynamics,
MNR & Guangxi/International Research Center on Karst, UNESCO, Guilin, Guangxi, 541004
[3]Pingguo Guangxi, Karst Ecosystem, National Observation and Research Station, Pingguo 531406, Guangxi, China

*Received: 25 March 2024*
*Accepted: 8 May 2024*

## Abstract

Highway construction in the karst areas of Guangxi has caused water- and soil-deficient rocky desertification slopes. Selecting plant species with high biomass and good drought tolerance is key for rapid vegetation recovery. This study measured two plant species' light and $CO_2$ response curves during extreme drought. At light saturation point ($I_{sat}$), the net photosynthetic rates ($P_n$) of *Pueraria lobata* (*P. lobata*) and *Bougainvillea spectabilis* (*B. spectabilis*) were low (4.14 and 2.38 μmol·m$^{-2}$·s$^{-1}$, respectively). Under drought conditions, they demonstrated distinct adaptive strategies. As irradiance increased, the water use efficiency (WUE), transpiration rate ($T_r$), and stomatal conductance ($G_s$) of *P. lobata* increased faster than those of *B. spectabilis*. As intercellular $CO_2$ concentration ($C_i$) increased, the measured maximum $P_n$ of *P. lobata* and *B. spectabilis* were 26.6 and 14.1 μmol·m$^{-2}$·s$^{-1}$, respectively. The $T_r$ and $G_s$ of *P. lobata* first decreased rapidly, then remained stable, while WUE increased linearly. However, $T_r$ and $G_s$ of *B. spectabilis* changed less, and WUE increased less than that of *P. lobata*. This shows that *P. lobata* can better adapt to water deficits and atmospheric $CO_2$ increases than *B. spectabilis*, with faster biomass accumulation. Measuring photosynthetic response characteristics is useful for quickly screening suitable plants for rocky desertified slope recovery.

**Keywords:** extreme drought, karst rocky desertification slope, light response curve, $CO_2$ response curve

## Abbreviation (In order of appearance in the text)

1. Light saturation point ($I_{sat}$)
2. net photosynthetic rates ($P_n$)
3. *Pueraria lobata* (*P. lobata)*
4. *Bougainvillea spectabilis (B. spectabilis)*
5. water use efficiency (WUE)
6. transpiration rate ($T_r$)
7. stomatal conductance ($G_s$)
8. intercellular $CO_2$ concentration ($C_i$)
9. $CO_2$ response curve ($A/C_i$ curve)
10. right-angle hyperbolic modified model (RHMM)
11. exponential model (EM)

*e-mail: huangfen@mail.cgs.gov.cn;
Tel.: +8615296002613;
Fax: +86773-5813708

12. right-angle hyperbolic model (RHM)
13. non-right-angle hyperbolic model (NRHM)
14. the maximum net photosynthetic rate ($P_{n\ max}$)
15. light compensation point ($I_c$)
16. dark respiration rate ($R_d$)
17. apparent quantum efficiency (AQE)
18. the Michaelis–Menten model (M-M)
19. the initial carboxylation efficiency (α)
20. $CO_2$ compensation point (Γ)
21. photorespiration rate ($R_p$)
22. coefficient of determination ($R^2$)
23. mean squared error (MSE)
24. mean absolute error (MAE)
25. photosynthetically active radiation (PAR)
26. $CO_2$ saturation point $C_{isat}$

## Introduction

The construction of highways in the karst areas of Guangxi inevitably leads to the creation of slopes due to excess soil excavation and the disposal of soil and debris. This directly damages mountain vegetation, causes severe soil erosion and a high rock exposure rate, and forms many rocky desertification slopes. Owing to poor site conditions and shallow, loose, backfilled soil, vegetation restoration of rocky desertification slopes is ineffective, with a low survival rate, maintenance difficulties, and high costs. Selecting plant species with high biomass and good drought resistance is crucial for achieving rapid vegetation restoration.

Previously, the screening of suitable plants primarily involved selecting dominant species in the local karst area and assessing their adaptability to drought stress and high-calcium environments [1]. This process involves various considerations, including morpho-anatomy, molecular physiological processes, and water utilization [2–4]. It is time-consuming and involves numerous indicators. Currently, there is no rapid and effective method to assess the suitability of alternative plants for specific environments, such as rocky desertification slopes along highways.

Understanding the photophysiological basis of photosynthesis and predicting photosynthetic trends under various environmental conditions is crucial for explaining crop productivity [5–7]. The quantitative relationship between the net photosynthetic rate ($P_n$) and photosynthetic effective radiation reveals the instantaneous response of plant photosynthetic physiological processes to environmental factors [8–10], termed the light response. This approach is the most effective for studying how the environment impacts plant photosynthesis. Specifically, the light-response curve model is ideal for evaluating the response of these plants to light. The corresponding physiological parameters can be obtained by analyzing the fitted light-response curve (light curve). Additionally, the $CO_2$ response curve ($A/C_i$ curve) of photosynthesis can be used to understand how photosynthesis responds to constantly changing environmental conditions [11, 12], and predict plant carbon absorption in future climate conditions [13, 14]. For example, the $A/C_i$ curve has been used efficiently to screen plants using bicarbonate radical ions [15]. These results raise questions about whether light response characteristics can be used to compare the suitability of alternative plants for karst rocky desertification environments and how their adaptive strategies differ.

This study focused on two plant species planted on rocky desertification slopes under arid conditions. Photosynthetic instruments were employed to measure the light curve and $A/C_i$ curve, and various models were utilized for fitting. Changes in the $P_n$ and water use efficiency (WUE) were analyzed, and differences in their light response characteristics were compared. Strategies for adapting to environmental change were analyzed, and pioneer species for rapid vegetation recovery were screened.

## Material and Methods

### Study Area

The research area was situated on the right slope of section No. 2 (YK296 + 300 – YK296 + 580) of the Laibin to Du'an highway, in Nongchang Village, Xincheng County, Laibin City, China. The slope extended over a length of 280 m, with a maximum vertical slope height of 26 m. The area was divided into three development levels, with a slope ratio of 1:1.75 for the first and second levels, and 1:2 for the third level. Active protective nets were employed for protection, along with the use of vines for greening purposes. Xincheng County is situated in a monsoon climate zone that transitions from subtropical to tropical regions, intersected by the Tropic of Cancer. The area experiences abundant sunshine and rainfall, with a mild climate. The terrain features erosion and hills, with ground elevations ranging from 145 to 180 meters and a relative height difference of 35 m. During autumn 2022, the area experienced minimal rainfall and severe drought conditions, as illustrated in Fig. 1. Between 17 September and 31 December 2022, the total rainfall amounted to 162 mm, with October recording only 17.8 mm of rainfall (Fig. 1).

### Experimental Species

The experimental species selected were the small shrub *Bougainvillea spectabilis* (*B. spectabilis*) and the vine *Pueraria lobata* (*P. lobata*), which were planted on a first-level slope in August 2022. *B. spectabilis* is widely employed as a landscape plant in Guangxi, while *P. lobata* is commonly utilized to enhance vegetation coverage on highway slopes. The soil was locally backfilled yellow lime soil, with a soil bulk density of 1.29±0.12 $g \cdot cm^{-3}$, soil mass moisture content ranging from 6.5% to 8.9%, salinity of 66.33±1.52 $ms \cdot m^{-1}$, pH of 6.56±0.23, total phosphorus of 0.23±0.01 $g \cdot kg^{-1}$, total potassium of 1.78±0.02 $g \cdot kg^{-1}$, and a cation exchange capacity of 4.98±0.06 $cmol \cdot kg^{-1}$.

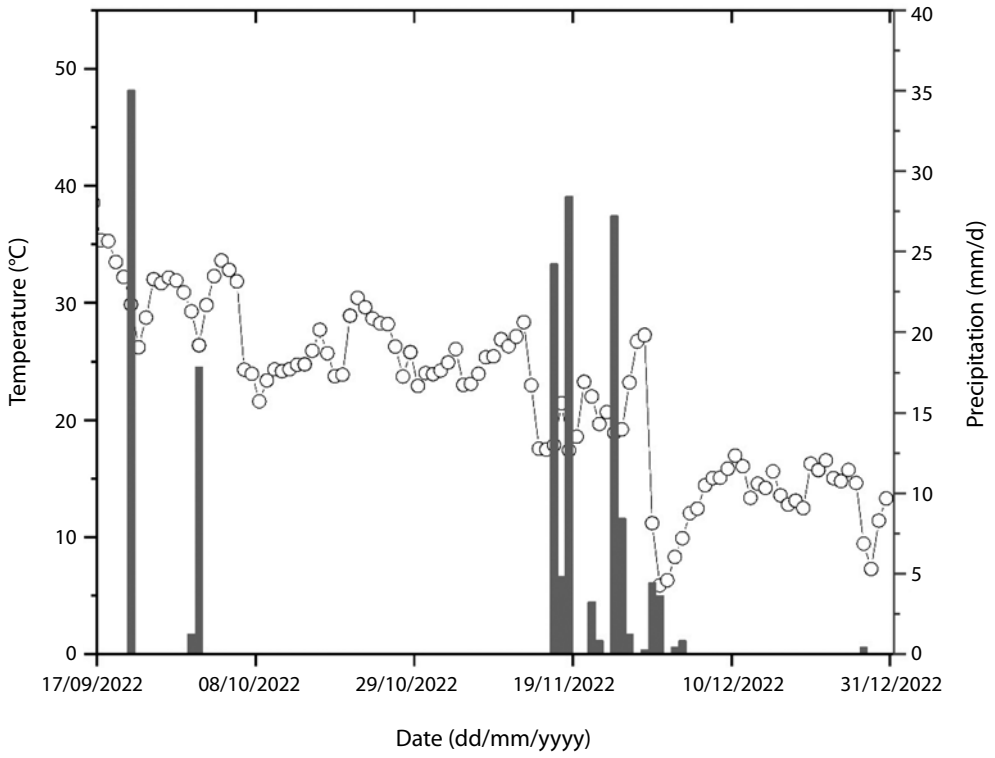


Fig. 1. Temperature and rainfall in the study area during the dry season.

The soil was characterized by aridity and barrenness. The sampling took place on 22–23 October 2022. During the dry season, the two plant species exhibit a decelerated growth rate without the manifestation of desiccation-induced leaf abscission or chlorosis.

## Light Curve Determination

Fully unfolded upper leaves were selected and a Li6400 portable photosynthesis instrument (LI-COR, Lincoln, NE, USA) was used from 08:00 to 11:30 to provide varying levels of photosynthetically active radiation through red and blue light sources. Radiation intensity was set to 2000, 1500, 1000, 800, 500, 300, 200, 150, 100, 50, 20, and 0 μmol $m^{-2}s^{-1}$ to assess the $P_n$ of the two plants under different light intensities. During measurements, the leaf temperature was set at 32°C, the gas source $CO_2$ concentration at 400 μ $mol \cdot mol^{-1}$, and the relative humidity at 18%. The experiment was conducted in triplicate, and the average value was reported with an error margin of < 10%. The gas flow rate was set at 500 $\mu mol \cdot s^{-1}$ and the photosynthetically active radiation was measured using automatic measurement mode, with a dwell time of 120–200 s at each set value. The measurement period was from 22 to 23 October 2022.

## $A/C_i$ Curve Determination

On a sunny morning, with a light saturation intensity of 1000 μmol/($m^2 \cdot s$) for *B. spectabilis* and 1250 $\mu mol \cdot m^{-2} \cdot s^{-1}$) for *P. lobata*, an airflow velocity of 500 $\mu mol \cdot s^{-1}$and a leaf surface temperature of 30°C, 13 $CO_2$ concentrations (400, 300, 200, 150, 100, 50, 400, 600, 800, 1000, 1200, 1600, and 2000 $\mu mol \cdot mol^{-1}$) were set for $CO_2$ response curve measurement. An automatic measurement mode was selected with a dwell time of 60–300 s at each set value. The $P_n$ of the two plants was measured and repeated three times, and the mean value of the three replicates was reported with an error margin of < 10%.

## Determination of Meteorological Indicators and Soil Physicochemical Properties

Temperature and rainfall were recorded using a self-recording rainfall collector (Davis 6466M, Davis Instruments, Hayward, CA, USA). Soil pH, bulk density, cation exchange capacity, total phosphorus, and total potassium were measured according to the methods described by Lu [16].

## Calculation and Analysis

The light curves of the tested plants were fitted and calculated using Photosynthesis Calculation software version 4.1.1, employing the right-angle hyperbolic modified model (RHMM), exponential model (EM), right-angle hyperbolic model (RHM), and non-right-angle hyperbolic model (NRHM) [17, 18]. Various indicators were calculated, such as the maximum net photosynthetic rate ($P_{n\ max}$), light compensation point ($I_c$), and dark respiration rate ($R_d$), along with other light response parameters and apparent quantum efficiency

(AQE). The $A/C_i$ curve of the tested plants was fitted and calculated using RHM, the Michaelis–Menten model (M-M), and RHMM [13, 14]. This analysis included calculating the initial slope of the $CO_2$ response curve, known as the initial carboxylation efficiency (α), along with response parameters such as $P_{n\,max}$, $CO_2$ compensation point (Γ), and photorespiration rate ($R_p$).

The coefficient of determination ($R^2$), mean squared error (MSE), and mean absolute error (MAE) were employed to assess the goodness of fit for each model. An $R^2$ value approaching 1 indicates a closer match between the predicted or fitted values and the measured values, reflecting higher model accuracy [19–21]. Photosynthetic Calculation software (version 4.1.1) was utilized to compute $R^2$ directly and the following formulas were applied to calculate MSE and MAE:

$$MSE = \frac{1}{n}\sum_{t=1}^{n}(y_t - \hat{y}_t)^2$$

$$MAE = \frac{1}{n}\sum_{t=1}^{n}|y_t - \hat{y}_t|$$

where $y_t$ and $\hat{y}_t$ represent the measured and fitted values, respectively. Origin 2020 software was used to statistically analyze and organize the data and draw charts.

## Results and Discussion

### Light Response Model Goodness of Fit Evaluation and Photosynthetic Parameters

The fitting results of the RHM, NRHM, RHMM, and EM for the light response of both species are presented in Table 1 and Fig. 2. The results indicate that, aside from the *B. spectabilis* RHM which exhibited a poor fit ($R^2 = 0.6076$), the fitting curves of other models for *B. spectabilis* and all four models for *P. lobata* demonstrated excellent agreement with the measured values ($R^2 > 0.96$). Except for the MSE and MAE values exceeding 1 for the *B. spectabilis* RHM, the MSE and MAE values for the other models were relatively small. Notably, EM for *B. spectabilis* exhibited the smallest MSE and MAE values, while NRHM for *P. lobata* demonstrated the smallest MSE and MAE values.

However, the methods used to estimate plant light saturation ($I_{sat}$) for these four light response models varied, leading to substantially different $I_{sat}$ (Fig. 3). The $I_{sat}$ value obtained for *B. spectabilis* using the NRHM model is notably lower than the measured value (Fig. 3). The $I_{sat}$ estimated by the RHM and RHMM models closely approximated the actual values. However, the $P_{n\,max}$ fitted by the RHM was 10, significantly higher than the measured value, whereas that estimated by the RHMM closely matched the observed value. Consequently, the larger the $R^2$ value, the higher the fitting degree of the light response model; however, the fitting results will not always match the measured values. Overall, the RHMM had the closest

Table 1. Photosynthetic parameters of light response curves for two plant species on rocky desertification slope during the dry season.

| Species | photosynthesis response model | Initial slope (α) | Maximum net photosynthetic rate ($P_{n\,max}$) | Light compensation point ($I_c$) | Light saturation point ($I_{sat}$) | Dark respiration rate ($R_d$) | $R^2$ | MSE | MAE |
|---|---|---|---|---|---|---|---|---|---|
| Bougainvillea spectabilis | RHM | 0.5883 | 10 | 28.3556 | 631.73 | -6.252 | 0.6076 | 3.011 | 1.287 |
| | NRHM | 0.0514 | 3.576 | 25.9924 | 247.06 | -1.2495 | 0.9889 | 0.014 | 0.094 |
| | RHMM | 0.0961 | 2.4308 | 20.6798 | 630.02 | -1.3597 | 0.9873 | 0.016 | 0.101 |
| | EM | 0.0417 | 2.2739 | 63.6628 | 151.84 | -1.5658 | 0.9933 | 0.009 | 0.07 |
| | Measurements | 0.0167 | 2.38 | 33.63 | 640 | -1.29 | / | / | / |
| Pueraria lobata | RHM | 0.0772 | 10 | 136.8526 | 520.73 | -5.1375 | 0.9871 | 0.121 | 0.309 |
| | NRHM | 0.0717 | 9.2687 | 134.0433 | 493.34 | -4.7193 | 0.9913 | 0.070 | 0.213 |
| | RHMM | 0.0656 | 4.6478 | 138.252 | 1505.02 | -4.5764 | 0.9909 | 0.072 | 0.211 |
| | EM | 0.0189 | 3.6036 | 175.1039 | 267.66 | -2.1679 | 0.9687 | 0.245 | 0.423 |
| | Measurements | 0.0267 | 4.135 | 176.93 | 1500.00 | -4.86 | / | / | / |

Note: right-angle hyperbolic model (RHM), non-right-angle hyperbolic model (NRHM), right-angle hyperbolic modified model (RHMM), exponential model (EM)

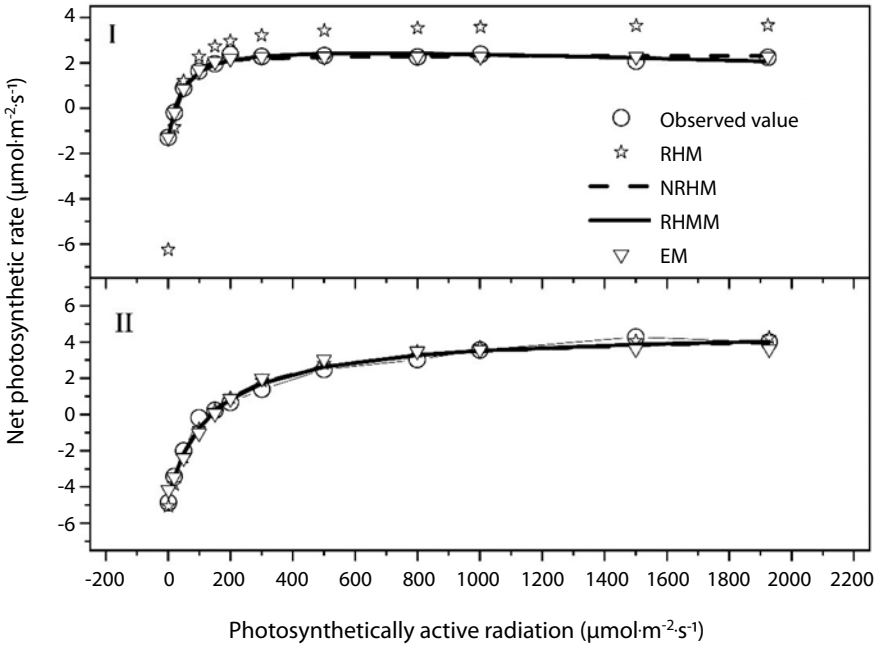


Fig. 2. Four models fitting the photosynthesis response curves of *B. spectabilis* (I) and *P. lobata* (II).

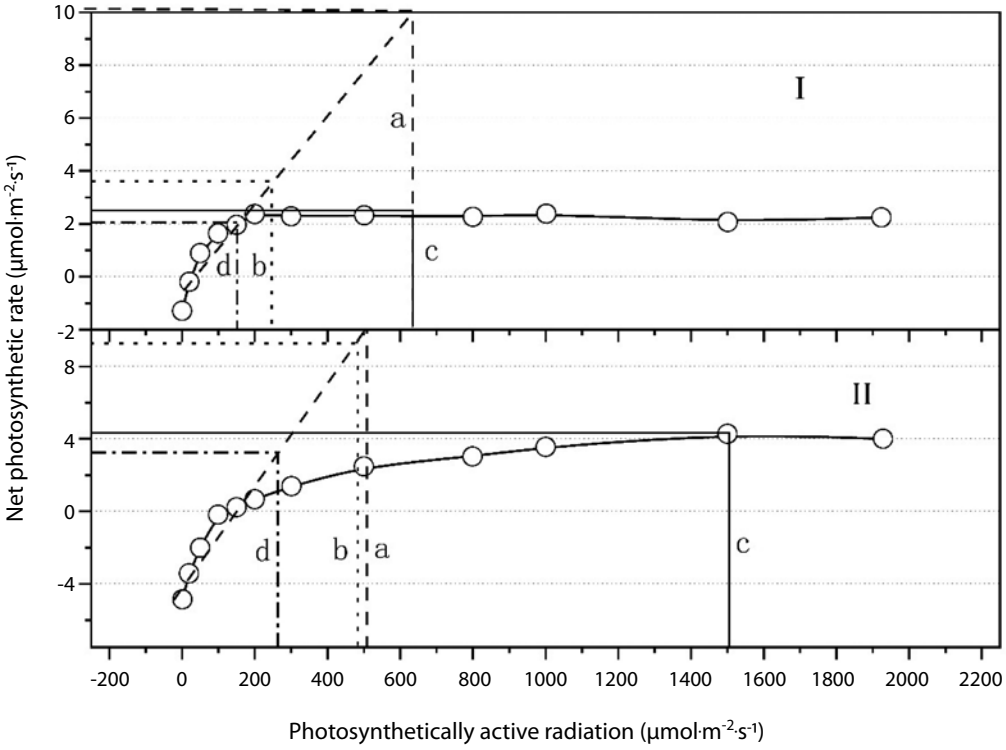


Fig. 3. Methods for estimating irradiance saturation ($I_{sat}$) using four photosynthesis response models.

a. RHM; b. NRHM; c. RHMM; d. EM assumes that the $I_{sat}$ is the photosynthetically active radiation (PAR) corresponding to a $P_{n\,max}$ of 0.9. The apparent quantum efficiencies (AQE) are the slopes of the linear fitting equations for the light response curve under PAR ≤ 200 μmol·m$^{-2}$·s$^{-1}$. a and b obtained the $I_{sat}$ by solving the linear equation $P_{n\,max} = AQE \times I_{sat} - R_d$ (dark respiration rate).

$I_{sat}$ and $P_{n\,max}$ to the measured values, with high fitting accuracy and the highest goodness of fit.

Similarly, the $I_{sat}$ obtained for *P. lobata* using the RHM, NRHM, and EM models were all notably lower than the measured values. In contrast, the $P_{n\,max}$ fitted by the RHM and NRHM were significantly higher than the measured values. Only the RHMM had an $I_{sat}$ and $P_{n\,max}$ close to the measured values ($R^2 = 0.99$; MSE and MAE ≤ 0.21). Overall, the RHMM had the highest degree of goodness of fit. Therefore, when evaluating the goodness of fit

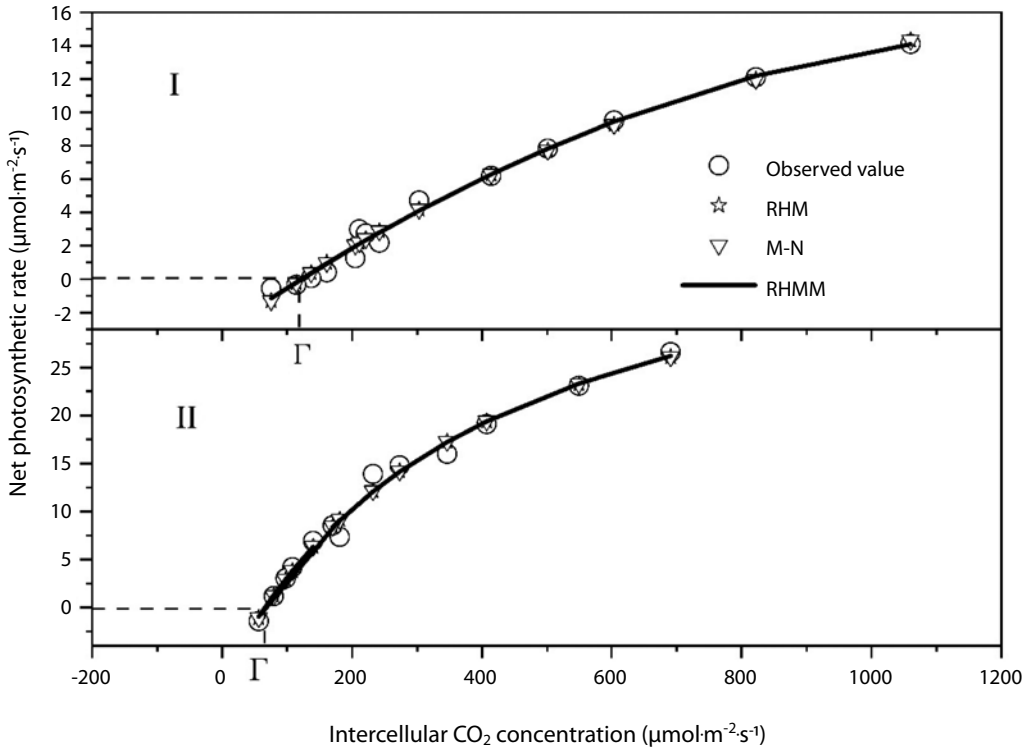


Fig. 4. $CO_2$ response curves of *B. spectabilis* and *P. lobata* for each model.

of various photoresponse models, it is important to consider not only their fitting effects but also their accuracy in fitting the data.

Given the optimality of the RHMM model, the data were compared using this model. The $P_{n\,max}$ of *P. lobata* was 48% higher than that of *B. spectabilis* (Table 1). $P_{n\,max}$ represents the peak photosynthetic capacity of leaves, indicating the maximum assimilation capacity achievable under specific environmental conditions [22]. The AQE of *B. spectabilis* and *P. lobata* were 0.0167 and 0.0267, respectively, with 37% higher in *P. lobata*. The AQE reflects the photosynthetic capacity of plants under low light conditions [18]. Previous studies showed that the range of AQY is from 0.03 to 0.05 in common plants under optimal conditions [10]. The AQE values are similar to those observed in *Mangifera indica* (0.020–0.024) [7] and slightly lower than those of *Populus euphratica* (0.036–0.044) [10], both under severe drought conditions.

For *P. lobata*, the $R_d$ was 29% higher than that of *B. spectabilis*, while the $I_c$ was 6.68 times higher and the $I_{sat}$ was 2.68 times higher than that of *B. spectabilis*. Overall, compared to *B. spectabilis*, *P. lobata* had a stronger ability to utilize both strong light and weak light. The *B. spectabilis* achieves organic compound preservation by minimizing dark respiration. Finally, *P. lobata* exhibits faster biomass growth under drought conditions and demonstrates a faster capability to cover exposed rocks on rocky slopes.

## $CO_2$ Response Model Goodness of Fit Evaluation and Photosynthetic Parameters

Fig. 4 shows the fitting results of the RHM, M-M, and RHMM models for the $CO_2$ responses of both species. The fitting curves of both species using the three models demonstrated agreement with the measured values ($R^2 > 0.98$). The $P_n$ values simulated by the RHM and M-M were consistent, with the RHM essentially being equivalent to the M-M model. The MSE and SAE of the RHMM for *B. spectabilis* were the smallest. From $P_{n\,max}$, the simulated values of the *B. spectabilis* RHMM were closest to the measured values (Table 2), whereas the RHM and M-M were far higher than the measured values, indicating a deviation from actual photosynthesis. The RHMM exhibited the best goodness of fit.

The RHM/M-M for *P. lobata* had the smallest MSE and SAE. For $P_{n\,max}$, the results of the three models were considerably higher than the measured values, with the RHMM displaying the smallest deviation from the measured values. Nevertheless, the fitting curve revealed that the measured values did not reach their maximum. Both the measured and fitted values increased with rising $CO_2$ concentration, and $P_n$ did not exhibit a decreasing or stable pattern, indicating that the $CO_2$ saturation point ($C_{isat}$) could not be identified.

The α value represents the slope of the line obtained by fitting the response data of $C_i \leq 200$ with a linear equation, reflecting both the quantity and enzymatic activity

Table 2. Photosynthetic parameters values of $CO_2$ response curves for two plant species on rocky desertification slope during the dry season.

| Species | $CO_2$ response model | Initial carboxylation slope (α) | $P_{n\,max}$ | $CO_2$ compensation point(Γ) | Photorespiration rate ($R_p$) | Coefficient of determination | MSE | SAE |
|---|---|---|---|---|---|---|---|---|
| *B. spectabilis* | RHM | 0.0323 | 37.5037 | 122.4672 | 3.5827 | 0.9888 | 0.233 | 0.405 |
| | MM | 0.0323 | 37.5037 | 122.4672 | 3.5827 | 0.9888 | 0.233 | 0.405 |
| | RHMM | 0.0269 | 14.8488 | 121.2775 | 3.1104 | 0.9899 | 0.212 | 0.364 |
| | Measurements | 0.0168 | 14.1 | 124.36 | / | / | | |
| *P. lobata* | RHM | 0.1407 | 52.4863 | 66.8315 | 7.9734 | 0.9895 | 0.668 | 0.569 |
| | MM | 0.1407 | 52.4863 | 66.8315 | 7.9734 | 0.9895 | 0.668 | 0.569 |
| | RHMM | 0.1345 | 45.2397 | 65.7786 | 7.5859 | 0.9894 | 0.672 | 0.581 |
| | Measurements | 0.0883 | 26.6 | 65.0058 | / | / | | |

of Rubisco [23]. The α values of *B. spectabilis* and *P. lobata* were 0.0168 and 0.0883, respectively, indicating that *P. lobata* had a higher cooperative ability under low $CO_2$ conditions. The $P_{n\,max}$, Γ, and $R_p$ of *P. lobata* were 1.89, 0.52, and 2.44 times higher than those of *B. Spectabilis* (Table 2), respectively. $P_{n\,max}$ reflects the activity of photosynthetic electron transfer and phosphorylation in plant leaves [24]. The Γ reflects the $CO_2$ concentration at which the rate of photosynthetic assimilation equals that of respiratory consumption in plant leaves [25]. This suggests that *P. lobata* had a stronger ability to utilize low and high $CO_2$ concentrations compared to *B. spectabilis*. Both the $R_p$ and the overall $P_n$ of *B. spectabilis* were higher (Table 2). Overall, *P. lobata* has a greater potential for biomass accumulation during a continuous increase in atmospheric $CO_2$ concentration.

The $C_{isat}$ reflects the ability of plants to utilize high $CO_2$ [26]. In contrast to previous studies, neither the measured nor simulated $C_i$ of *P. lobata* reached saturation. Zhu et al. [21] found that under different nitrogen conditions, $P_n$ gradually increased and eventually stabilized as the $CO_2$ concentration increased. However, Arp [27] observed that two Chinese *Liriodendron* plants grown at high $CO_2$ concentrations for an extended period did not reach saturation, resulting in significant changes in the $C_{isat}$ of the plants grown under high $CO_2$ concentrations. In this study, *P. lobata* lived under extreme drought conditions for an extended period, preventing it from reaching the $C_{isat}$; however, the rate of increase gradually decreased. Photosynthesis under light saturation is constrained by its carboxylation ability at low $CO_2$ levels and by electron transfer and ribulose bisphosphate regeneration at high $CO_2$ levels [25].

## RHMM is the Best Fitting Model for the Light and $CO_2$ Response Curves

Researchers have established various response models of photosynthesis, including common light response models such as RHM, NRHM, EM, and RHMM [28]. Previous studies [7, 10] found that the RHMM can better estimate $I_{sat}$ than other models. This model simulates functions with extreme values and high accuracy, resulting in a fitting effect closer to the actual values compared to other models, particularly applicable to arid desert habitats [10].

The RHMM was also the optimal model for the light and $CO_2$ response curves in our results. Fitting the light-response curve offers two advantages: firstly, it can directly calculate the $I_{sat}$ and the $P_{n\,max}$ of plants. Secondly, it allows for the fitting of light response curves of plants under two conditions: either no decrease in $P_n$ after reaching $I_{sat}$ or decreased photosynthetic rate. The estimated $I_{sat}$ and $P_{n\,max}$ were closest to the measured values [7, 10, 26].

Similarly, during the fitting of the $CO_2$ response curve, neither the RHM nor the M-M models were able to fully capture the decline in $P_n$ with increasing $CO_2$, nor could they accurately estimate $P_{n\,max}$. The RHMM demonstrated a good fit with an $R^2$ value and outperformed the other models in terms of fit. Its photosynthetic parameters, including α, the fitted $P_{n\,max}$ values, and $C_{isat}$, closely approximated the true values and accurately reflected the actual situation.

## Light Response and A/Ci Curves of Transpiration Rate ($T_r$), WUE, Stomatal Conductance ($G_s$), and Intercellular $CO_2$ Concentration ($C_i$)

A positive linear relationship was observed between $T_r$, $G_s$, and photosynthetically active radiation (PAR). WUE rapidly increased from 0 to 250 $\mu mol \cdot m^{-2} \cdot s^{-1}$ of PAR and subsequently stabilized. Contrary to the $P_n$, $C_i$ exhibited a rapid decline from 0 to 250 $\mu mol \cdot m^{-2} \cdot s^{-1}$ of PAR before stabilizing (Fig. 5). The $G_s$ of *B. spectabilis* remained relatively stable, whereas WUE exhibited a slight decrease after reaching its peak value (Fig. 5). The rapid decline in $C_i$ indicates a high demand for raw photosynthetic $CO_2$ and high photosynthetic efficiency. Due to the small

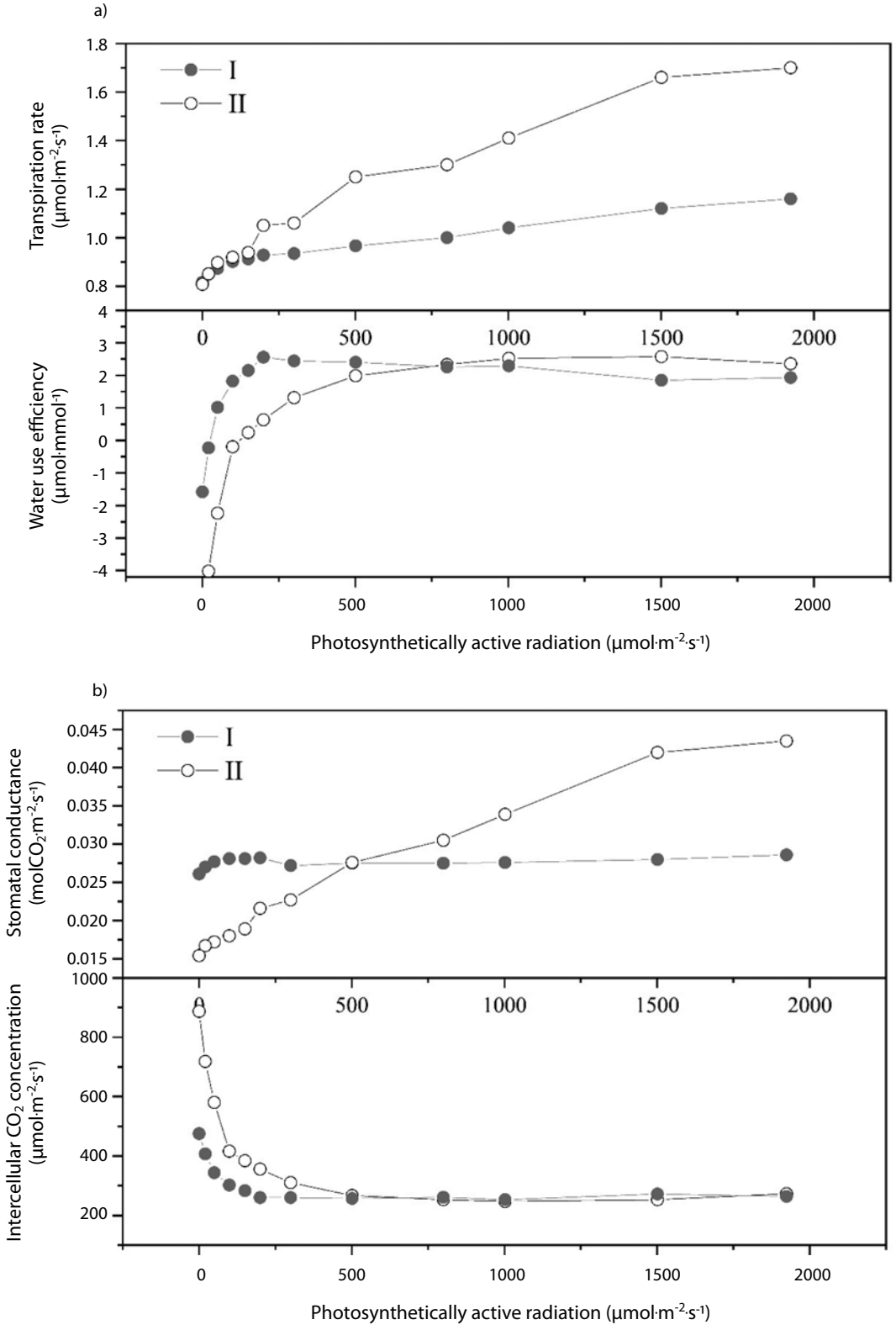


Fig. 5. Photosensitive curves of transpiration rate ($T_r$), water use efficiency (WUE), stomatal conductance ($G_s$), and intercellular $CO_2$ concentration ($C_i$).

increase in $G_s$ under low-light conditions, the increased photosynthetic rate rapidly increased $CO_2$ consumption, leading to decreased $CO_2$ levels [5].

Under weak light conditions (0–250 μmol·m$^{-2}$·s$^{-1}$), *B. spectabilis* had higher WUE and $G_s$ compared to *P. lobata*, resulting in a higher $P_n$ and lower $C_i$ (Fig. 4). As the PAR increased, the $T_r$, WUE, and $G_s$ of *P. lobata* rapidly increased, whereas the corresponding rise in *B. spectabilis* was slower. Consequently, this resulted in a rapid increase in the $P_n$ of *P. lobata*, surpassing that

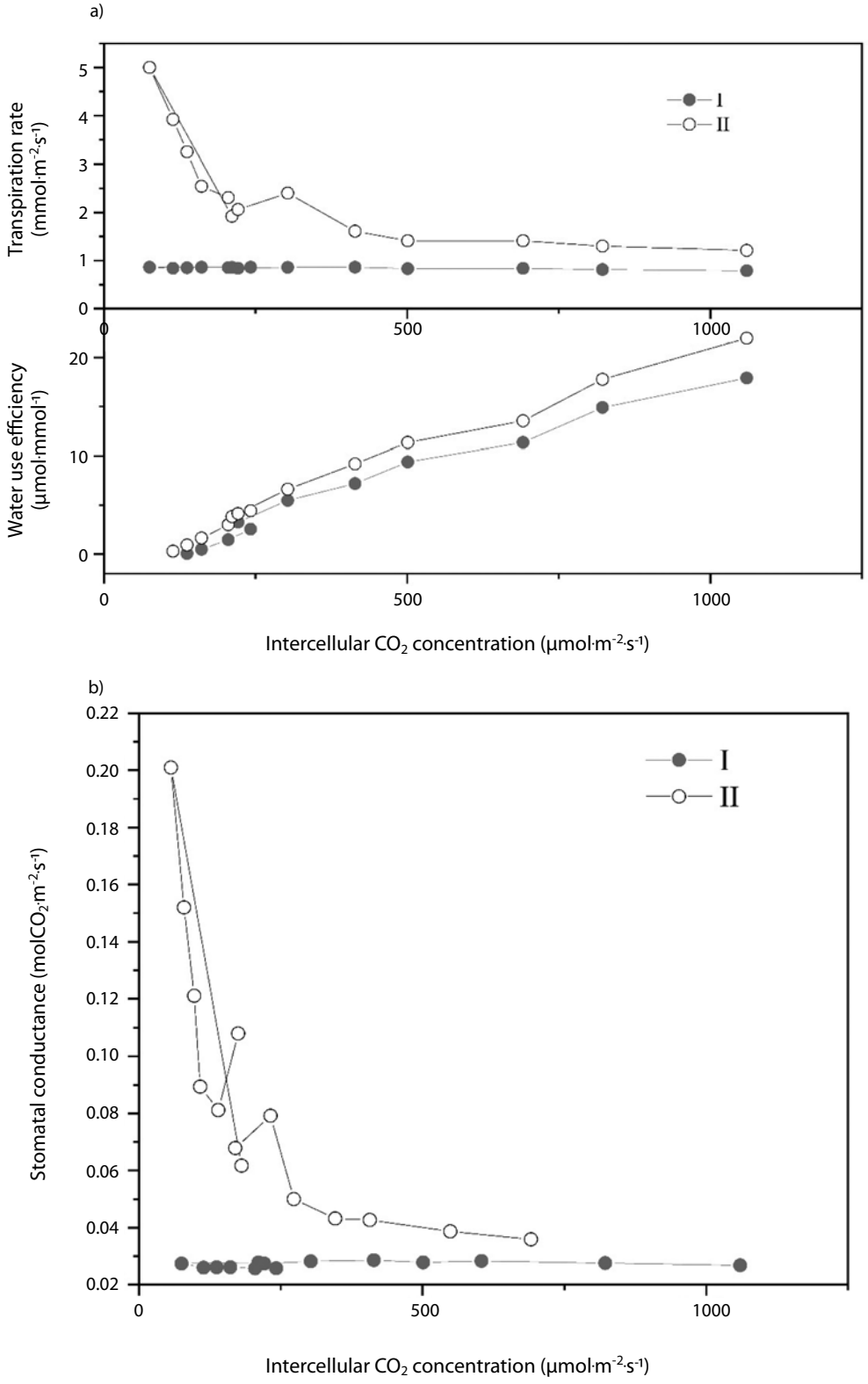


Fig. 6. $CO_2$ response curves of $T_r$, WUE, and $G_s$.

of *B. spectabilis*, and a rapid decrease in $C_i$ (Fig. 5). Under drought conditions, the two species exhibit distinct adaptive strategies. *B. spectabilis* employs a lower organic matter decomposition rate (lower $R_d$) and maintains stable $G_s$ to reduce organic matter consumption and excessive water transpiration. However, solely enhancing WUE leads to a slight increase in $P_n$. This can be compared to the strategy of deciduous plants shedding leaves to reduce transpiration and entering a dormant state throughout the entire drought period [29]. In contrast, The *P. lobata* responds actively

to increased light levels by augmenting $G_s$, $T_r$, and WUE, thereby enhancing the rate of organic matter accumulation, and exhibiting a performance similar to non-water-stressed state [5].

WUE in both *B. spectabilis* and *P. lobata* was positively correlated with $C_i$. The $T_r$ and $G_s$ of *P. lobata* rapidly decreased at $C_i$ levels between 0–250 μmol·m$^{-2}$·s$^{-1}$, followed by a slower decline (Fig. 6). The higher concentration of $CO_2$ enables plants to engage in photosynthesis more efficiently, thereby reducing the demand for stomatal opening. By reducing stomatal aperture, plants can effectively regulate water balance and decrease transpiration rates in environments with elevated $CO_2$ concentrations [30]. Meanwhile, *B. spectabilis* consistently maintains lower $G_s$ and $T_r$ to minimize water consumption (Fig. 6).

### Indicative Significance of *P. lobata* and *B. spectabilis* in Response to Environmental Changes

Research indicates that water stress significantly impacts the light response of *Cucumis sativus* leaves, leading to a reduction in their photosynthetic capacity [21]. Water stress not only reduced gas exchange parameters, such as $G_s$, $T_r$, and WUE of *Bothriochloa ischaemum,* but also reduced the parameters of the $P_n$-PAR curves, such as $P_n$, AQE, and $I_c$. Water serves as the primary limiting factor for photosynthesis in *B. ischaemum*, and appropriate nitrogen application can enhance its potential photosynthetic capacity under water-deficient conditions [31]. When the relative soil moisture content falls below the optimal range, $P_n$ and plant growth decrease significantly by influencing various cellular and physiological processes [32, 33]. Therefore, under severe drought conditions, the $P_{n\,max}$ of *B. spectabilis* (2.38 μmol·m$^{-2}$·s$^{-1}$) and *P. lobata* (4.14 μmol·m$^{-2}$·s$^{-1}$) in this study were lower compared to *Bidens pilosa* (6.5 μmol·m$^{-2}$·s$^{-1}$), P. *euphratica* (8.41–12.60 μmol·m$^{-2}$·s$^{-1}$) [10] and *Mangifera indica* (3.45–3.97 μmol·m$^{-2}$·s$^{-1}$) [7].

Under low irradiance, photosynthesis is limited by the electron transfer rate, while under high irradiance, photosynthesis is often limited by Rubisco activity [34]. Consequently, as the light intensity gradually increased, the $P_n$ of *B. spectabilis* and *P. lobata* also increased gradually and then stabilized after reaching the $I_{sat}$.

Generally, for species with C3 photosynthesis, elevated $CO_2$ leads to a 50% increase in $P_n$ [35], and a 157% increase in plant biomass and leaf area [36]. Free-air $CO_2$ enrichment technology developed recently [37, 38] can increase the $CO_2$ concentration by 150% under field conditions, resulting in a 31% increase in the photosynthesis rate and an approximately 18% increase in crop yield [25, 39–41]. Although short-term exposure to elevated atmospheric $CO_2$ can lead to a significant increase in photosynthesis in many plants, long-term growth in elevated $CO_2$ typically results in a smaller increase in photosynthesis owing to reduced photosynthetic capacity [37, 38].

In the face of future frequent, extreme droughts and continuously increasing $CO_2$ concentrations, *P. lobata* is expected to exhibit better adaptation to changing water availability and atmospheric $CO_2$ levels than *B. spectabilis*; it maintained a higher photosynthesis rate and faster biomass accumulation, rendering it a superior species choice for restoring rocky desertification slopes. However, *B. spectabilis* is capable of surviving and maintaining a lower growth rate under drought conditions by retaining lower $G_s$ and transpiration rates, thus fulfilling the landscape requirements of highways. Integrating vine and shrub planting in vegetation configuration contributes to soil and water conservation on rocky desertification slopes and enhances ecosystem stability [42]. Measuring the photosynthetic response of plants is a rapid method for screening plants suitable for this purpose. It should be noted that the challenges associated with capturing the extreme arid climate conditions resulted in the small sample size, short study period, and lack of replication of this study at different sites. These limitations could be addressed in future studies by expanding the sample size and conducting studies across multiple sites with similar conditions or using indoor simulations.

## Conclusions

(1) The RHMM is the most effective model for *P. lobata* and *B. spectabilis* light and $CO_2$ response curves under severe water deficit conditions. It can simulate the stabilization or decline of the $P_n$ after reaching the $I_{sat}$, with simulated values closely approximating the true values compared to other models.

(2) Under drought conditions, *P. lobata* and *B. spectabilis* demonstrate distinct adaptive strategies. *B. spectabilis* enhances WUE, resulting in a slight increase in $P_n$ response to elevated PAR and $CO_2$. It maintains stable $G_s$ and $T_r$ to mitigate organic matter consumption and excessive water transpiration. In contrast, *P. lobata* responds actively to increased PAR by increasing $G_s$, $T_r$, and WUE. Meanwhile, *B. spectabilis* reduces $G_s$ and $T_r$ to minimize water consumption while enhancing WUE to promote a higher organic matter accumulation rate.

(3) *P. lobata* responded faster to light and $CO_2$ changes and exhibited higher WUE. Therefore, it could better adapt to changes in water availability and atmospheric $CO_2$ increases than *B. spectabilis*, making it a superior choice for restoring rocky desertification slopes. Consequently, simultaneous measurement of the photosynthetic response characteristics of plants provides a rapid and effective method for species selection in rocky desertification slope restoration.

## Acknowledgments

This study was funded by the Natural Science Foundation of Guangxi (No. 2022GXNSFAA035569, Guike-AD21196001), the Project of the China Geological Survey (No. DD20230547), Key Science and Technology Projects in Guangxi Transport Industry (GXHS-2022-016), and the Guilin Science Research and Technology Development Plan Project (2020010905).

## Conflict of Interest

The authors declare no conflict of interest.

## References


1. GUO K., LIU C., DONG M. Ecological adaptation of plants and control of rocky-desertification on karst region of South-west China. Chinese Journal of Plant Ecology, **35** (10), 991, **2011** [in Chinese].
2. FAN B., XIONG K.N., LIU Z.Q. Forest Plant Water Utilization and the Eco-Hydrological Regulation in the Karst Desertification Control Drainage Area. Forests, **14** (4), 747, **2023**.
3. YANG Q., ZHU D.Y., CHEN J. Effects of Planting Patterns on Soil Aggregates and Enzyme Activities in Rocky Desertification Areas of Karst Plateau Mountains. Polish Journal of Environmental Studies, **32** (1), 405, **2023**.
4. SONG T., HUANG C., YANG H., LIANG J.H., MA Y.Q., XU C., LI M.B., LIU X., ZHANG L.K. Characterization of Soil-Plant Leaf Nutrient Elements and Key Factors Affecting Mangoes in Karst Areas of Southwest China. Land, **11** (7), 970, **2022**.
5. LI T., WANG P., LI Y., LI L., KONG R., FAN W., YIN W., FAN Z., WU Q., ZHAI Y. Effects of Configuration Mode on the Light-Response Characteristics and Dry Matter Accumulation of Cotton under Jujube–Cotton Intercropping. Applied Sciences, **13** (4), 2427, **2023**.
6. SERDIO J., MOREIRA D., BASTOS A., CARDOSO V., FROMMLET J., FRANKENBACH S. Hysteresis light curves: a protocol for characterizing the time dependence of the light response of photosynthesis. Photosynthesis Research, **154** (1), 57, **2022**.
7. LI Y.L., LIU X.G., HAO K., YANG Q.L., YANG X.Q., ZHANG W.H., CONG Y. Light-response curve of photosynthesis and model fitting in leaves of under different soil water conditions. Photosynthetica, **57** (3), 796, **2019**.
8. ELFADL M.A., LUUKKANEN O. Field studies on the ecological strategies of Prosopis juliflora in a dryland ecosystem: 1. A leaf gas exchange approach. Journal of Arid Environments, **66** (1), 1, **2006**.
9. GOVINDJEE, KROGMANN D. Discoveries in oxygenic photosynthesis (1727–2003): a perspective. Springer Netherlands, **80** (1-3), 15, **2004**.
10. WANG H., HAN L., XU Y., NIU J., YU J. Simulated photosynthetic responses of Populus euphratica during drought stress using light-response models. Acta Ecologica Sinica, **37** (7), 2315, **2017** [in Chinese].
11. SLOT M., WINTER K. Photosynthetic acclimation to warming in tropical forest tree seedlings. Journal of Experimental Botany, **68** (9), 2275, **2017**.
12. SMIT N.G., DUKES J.S. Short-term acclimation to warmer temperatures accelerates leaf carbon exchange processes across plant types. Global Change Biology, **23** (11), 4840, **2017**.
13. OLESON K.W., LAWRENCE D.M., BONAN G.B., FLANNER M.G., ZENG X. Technical Description of version 4.0 of the Community Land Model (CLM). National Center for Atomospheric Research, Boulder, Colarado, **2010**.
14. STINZIANO J.R., ADAMSON R.K., HANSON D.T. Using multirate rapid A/Ci curves as a tool to explore new questions in the photosynthetic physiology of plants. New Phytologist, **222** (2), 785, **2019**.
15. WU Y., HANG H., ZHAO K., XING D., LIANG Z., XIE T., LI H., LIU Y. Method for screening plants using bicarbonate radical ions efficiently by using photosynthetic carbon dioxide response curve. China, **2014**.
16. LU R. Soil agricultural chemical analysis method. Agricultural science and technology press of China, Beijing, **2000** [in Chinese].
17. HAN G., ZHAO Z. Light response characteristics of photosynthesis of four xerophilous shrubs under different soil moistures. Acta Ecologica Sinica, **30** (15), 4019, **2010** [in Chinese].
18. YE Z., YU Q. Comparison of new and several classical models of photosynthesis in response to irradiance. Chinese Journal of Plant Ecology, **32** (6), 1356, **2008** [in Chinese].
19. CHEN Z., PENG Z., YANG J., CHEN W., OU-YANG Z. A mathematical model for describing light-response curves in Nicotiana tabacum L. Photosynthetica, **49**, 467, **2011**.
20. LIU J., LUO J., LI R., WANG J., LIU J. Fitting and Analysis of Light Response Curve of Phoebe zhennan Seedlings in Karst Vertical Heterogeneous Habitats Under Different Rainfall Time Patterns. Journal of Southwest University (Natural Science Edition), **45** (3), 122, **2023** [in Chinese].
21. ZHU X., JIA M., SHI P., YANG C., BAI Y.-X., ZHANG H., LYU F., WANG G. Fitting analysis of $CO_2$ response curve of tobacco under different nitrogen fertilizer levels. Journal of Southern Agriculture, **51** (3), 537, **2020** [in Chinese].
22. KROMDIJK J., GLOWACKA K., LEONELLI L., GABILLY S.T., IWAI M., NIYOGI K.K., LONG S.P. Improving photosynthesis and crop productivity by accelerating recovery from photoprotection. Science, **354** (6314), 857, **2016**.
23. DRIEVER S.M., SIMKIN A.J., ALOTAIBI S., FISK S.J., MADGWICK P.J., SPARKS C.A., JONES H.D., LAWSON T., PARRY M.A.J., RAINES C.A. Increased SBPase activity improves photosynthesis and grain yield in wheat grown in greenhouse conditions. Philosophical Transactions of the Royal Society Biological Sciences, **372** (1730), **2017**.
24. YE Z., YU Q. A coupled model of stomatal conductance and photosynthesis for winter wheat. Photosynthetica, **46** (4), 637, **2008**.
25. BUSCH F.A., SAGE R.F. The sensitivity of photosynthesis to $O_2$ and $CO_2$ concentration identifies strong Rubisco control above the thermal optimum. New Phytologist, **213** (3), 1036, **2017**.
26. YE Z., YU F., AN T., WANG F., KANG H. Investigation on $CO_2$-response model of stomatal conductance for plants. Chinese Journal of Plant Ecology, **45** (4), 420, **2021** [in Chinese].
27. ARP W.J., DRAKE B.G. Increased photosynthetic capacity of Scirpus olneyi after 4 years of exposure to elevated $CO_2$. Plant, Cell & Environment, **14** (9), 1003, **1991**.
28. YE Z. A new model for relationship between irradiance and the rate of photosynthesis in Oryza sativa. Photosynthetica, **45** (4), 637, **2007**.
29. CHEN Z.C., LI S., WAN X.C., LIU S.R. Strategies of tree species to adapt to drought from leaf stomatal regulation and stem embolism resistance to root properties. Frontiers in Plant Science, **13**, **2022**.
30. CHANG Z.J., HAO L.H., LU Y.Z., LIU L., CHEN C.H., SHI W., LI Y., WANG Y.R., TIAN Y.S. Effects of elevated $CO_2$ concentration and experimental warming on morphological, physiological, and biochemical responses

of winter wheat under soil water deficiency. Frontiers in Plant Science, **14**, **2023**.
31. XU W., DENG X., XU B. Effects of water stress and fertilization on leaf gas exchange and photosynthetic light-response curves of Bothriochloa ischaemum L. Photosynthetica, **51** (4), 603, **2013**.
32. BEN MHENNI N., SHINODA M., NANDINTSETSEG B. Assessment of drought frequency, severity, and duration and its impacts on vegetation greenness and agriculture production in Mediterranean dryland: A case study in Tunisia. Natural Hazards, **105** (3), 2755, **2021**.
33. OZDEMIR D. The impact of climate change on agricultural productivity in Asian countries: a heterogeneous panel data approach. Environmental Science and Pollution Research, **29** (6), 8205, **2022**.
34. ÖGREN E., EVANS J. Photosynthetic light-response curves: I. The influence of CO2 partial pressure and leaf inversion. Planta, **189** (2), 182, **1993**.
35. HAO L.H., CHANG Z.J., LU Y.Z., TIAN Y.S., ZHOU H.R., WANG Y.R., LIU L., WANG P., ZHENG Y.P., WU J.Y. Drought dampens the positive acclimation responses of leaf photosynthesis to elevated $CO_2$ by altering stomatal traits, leaf anatomy, and Rubisco gene expression in. Environmental and Experimental Botany, **211**, **2023**.
36. WANG L., ZHENG J.P., WANG G.R., DANG Q.L. Combined effects of elevated $CO_2$ and warmer temperature on limitations to photosynthesis and carbon sequestration in yellow birch. Tree Physiology, **43** (3), 379, **2023**.
37. POORTER H., FIORANI F., PIERUSCHKA R., WOJCIECHOWSKI T., VAN DER PUTTEN W.H., KLEYER M., SCHURR U., POSTMA J. Pampered inside, pestered outside? Differences and similarities between plants growing in controlled conditions and in the field. New Phytologist, **212** (4), 838, **2016**.
38. BATKE S.P., YIOTIS C., ELLIOTT-KINGSTON C., HOLOHAN A., MCELWAIN J. Plant responses to decadal scale increments in atmospheric $CO_2$ concentration: comparing two stomatal conductance sampling methods. Planta, **251** (2), **2020**.
39. KIMBALL B.A. Crop responses to elevated $CO_2$ and interactions with $H_2O$, N, and temperature. Current Opinion in Plant Biology, **31**, 36, **2016**.
40. AINSWORTH E.A., LONG S.P. 30 years of free-air carbon dioxide enrichment (FACE): what have we learned about future crop productivity and its potential for adaptation? Global Change Biology, **27** (1), 27, **2021**.
41. POORTER H., KNOPF O., WRIGHT I.J., TEMME A.A., HOGEWONING S.W., GRAF A., CERNUSAK L.A., PONS T.L. A meta-analysis of responses of C3 plants to atmospheric $CO_2$: dose–response curves for 85 traits ranging from the molecular to the whole-plant level. New Phytologist, **233** (4), 1560, **2022**.
42. CAO W., ZHU N., MENG Z., LV C., CHEN Y., WANG G. Linking Vegetation Diversity and Soils on Highway Slopes: A Case Study of the Zhengzhou–Xinxiang Section of the Beijing–Hong Kong–Macau Highway. Forests, **14** (9), 1863, **2023**.